Bioelectrochemistry 134 (2020) 107540

Contents lists available at ScienceDirect

Bioelectrochemistry

journal homepage: www.elsevier.com/locate/bioelechem

Covalent immobilization of delipidated human serum albumin on poly (pyrrole-2-carboxylic) acid film for the impedimetric detection of perfluorooctanoic acid

Giulia Moro [a,b,c,*,1], Fabio Bottari [b,c,1], Stefano Liberi [a], Sonia Covaceuszach [d], Alberto Cassetta [d], Alessandro Angelini [a,e], Karolien De Wael [b,c], Ligia Maria Moretto [a]

[a] Department of Molecular Sciences and Nanosystems, Ca' Foscari University of Venice, Via Torino 155, 30172 Mestre, Italy
[b] AXES Research Group, Department of Bioscience Engineering, University of Antwerp, Groenenborgerlaan 171, 2020 Antwerp, Belgium
[c] NANOlab Center of Excellence, Groenenborgerlaan 171, 2020 Antwerp, Belgium
[d] Istituto di Cristallografia – CNR, Trieste Outstation, Italy SS 14 km 163.5, Basovizza, Trieste, Italy
[e] European Centre for Living Technology (ECLT), Ca' Bottacin, Dorsoduro 3911, Calle Crosera, 30123 Venice, Italy

ARTICLE INFO

Article history:
Received 27 February 2020
Received in revised form 20 April 2020
Accepted 20 April 2020
Available online 26 April 2020

Keywords:
Pyrrole-2-carboxylic acid
Impedimetric sensor
Biosensor
Electropolymerization
Perfluorooctanoic acid
Human serum albumin

ABSTRACT

The immobilization of biomolecules at screen printed electrodes for biosensing applications is still an open challenge. To enrich the toolbox of bioelectrochemists, graphite screen printed electrodes (G-SPE) were modified with an electropolymerized film of pyrrole-2-carboxilic acid (Py-2-COOH), a pyrrole derivative rich in carboxylic acid functional groups. These functionalities are suitable for the covalent immobilization of biomolecular recognition layers. The electropolymerization was first optimized to obtain stable and conductive polymeric films, comparing two different electrolytes: sodium dodecyl sulphate (SDS) and sodium perchlorate. The G-SPE modified with Py-2-COOH in 0.1 M SDS solution showed the required properties and were further tested. A proof-of-concept study for the development of an impedimetric sensor for perfluorooctanoic acid (PFOA) was carried out using the delipidated human serum albumin (hSA) as bioreceptor. The data interpretation was supported by size exclusion chromatography and small-angle X-ray scattering (SEC-SAXS) analysis of the bioreceptor-target complex and the preliminary results suggest the possibility to further develop this biosensing strategy for toxicological and analytical studies.

1. Introduction

Electrochemical sensors and biosensors are answering the increasing need of portable tools for the semi-quantitative detection of environmental contaminants (EC) by direct electrochemical fingerprinting or indirect sensing strategies [1]. In the broader context of EC, per- and polyfluoroalkyl substances (PFAS) represent a class of chemicals in continuous expansion (see emerging PFAS in [2,3]). PFAS and particularly perfluorooctanoic acid (PFOA) are still subjected to extensive toxicological studies to clarify their effects on the ecosystem and human health [4]. Nonetheless, previous studies already claimed their tendency to undergo bioaccumulation in vegetal and animal tissues [5] suggesting the need of large-scale, strict monitoring plans [6] and efficient water treatments [7]. For these reasons, there is an urgent demand of novel sensors for natural and industrial water monitoring, which needs to be rapid, user-friendly, robust and sensitive enough to reach the legislation limits of such EC. Electrochemical biosensors have been regarded as one of the most promising alternative to meet analogous demands in several other fields, such as point-of-care testing [8] and food safety [9].

Concerning the detection of PFOA, only few examples of electrochemical sensors have been reported up to now, mainly potentiometric [10], electrochemiluminescence [11] and photoelectrochemical [12] ones. These sensors are all based on biomimetic receptors such as the molecularly imprinted polymers (MIP) employed also in PFOA removal [13] and non-electrochemical sensing devices [14]. However, also bioreceptors can play an important role in PFOA sensing, as showed by the immunosensor developed by Cennamo *et al.* [15]. So far, protein-based bioreceptor have not been considered, although serum proteins-PFAS interactions were largely investigated [16]. In particular, PFOA capability to interact

* Corresponding author.
E-mail address: giulia.moro@unive.it (G. Moro).
[1] These authors contributed equally to this work and should be considered co-first authors.

https://doi.org/10.1016/j.bioelechem.2020.107540
1567-5394/

with albumin (thanks to PFOA fatty-acid mimic behaviour) was clearly stated in numerous toxicological studies [17,18] giving the opportunity to use these common proteins as a bioreceptors for PFOA sensing. Moreover, albumin-based electrochemical sensors have already showed good performances in the highly selective and sensitive detection of small molecules [19] as well as larger targets [20]. Albumin is non-electroactive and often combined with impedimetric affinity-based sensors, where the bioreceptor is first immobilized on the electrode surface, detecting the protein-target interaction as a localized change in the electrode-solution interface [21]. However, the immobilization of the bioreceptor is usually a bottleneck in the development of new sensors, particularly at screen printed electrode. To overcome this issue, other surface modifiers are often included to guarantee the stability of the immobilization as well as the electrode surface conductivity and consequently the device sensitivity. Zamani *et al.* [22] recently reviewed the preeminent role of conductive electropolymerized polymers, especially pyrrole and its derivatives, that were extensively studied and applied as electrode modifiers [23]. Among the pyrrole derivates, pyrrole-2-carboxylic acid (Py-2-COOH) was less employed in electroanalytical applications [24–26], even possessing many sought-after characteristics compared to the parent compound pyrrole, such as the presence of the carboxylic acid functional groups which can be used to couple amide-bearing molecules to the surface via EDC/NHS chemistry. The complete characterization of the electrochemical polymerization pathway of Py-2-COOH has been previously reported [27]. The results obtained by Foschini *et al.* [27] allowed to conclude that the electropolymerization mechanism is very similar to the one of pyrrole, as reported by Dias *et al.* [28]. The final polymeric chain will present a torsion angle between subsequent monomeric units of 74°, compared to 54° of pyrrole [27]. Thus, the electropolymerization conditions already reported and studied for pyrrole can also be applied to the polymerization of Py-2-COOH. Considering the specific electron transfer properties of polypyrrole, the conductivity of the resulting film is influenced by the electrolyte in which the electropolymerization takes place [28]. The polypyrrole film is doped with about 20–30% of anions coming from the electrolyte, and the conductivity is linked to the exchange of trapped anions between the film and the solution [29]. Moreover, acid anions increase the conductivity, while basic ones decrease it [30]. Also the size of the anion is important for the growth of the film and its performances, such as stability to overoxidation [31]. All these parameters need to be taken into account to design suitable poly(Py-2-COOH) modification protocol compatible with graphite screen-printed electrodes (G-SPE).

Aiming to obtain stable and conductive poly(Py-2-COOH) on the electrode surface for the covalent immobilization of biomolecules, we first optimized the main electropolymerization parameters based on previously reported data [32–34]. In particular, the comparison of two different electrolytes, one organic (SDS) and another inorganic ($NaClO_4$), allowed understanding the influence of the anions on the conductivity of the obtained films at G-SPE. The optimized poly(Py-2-COOH) was then tested in an impedimetric biosensing platform. Delipidated human serum albumin (hSA) was selected as bioreceptor for PFOA sensing. The delipidation treatment, removing the fatty acids embedded in the protein, increase the available bindings site for PFOA [35], improving also the batch-to-batch reproducibility of the bioreceptor. The binding event was followed by electrochemical impedance spectroscopy (EIS) and the changes in the hSA-PFOA complex conformation were verified by SEC-SAXS (Size Exclusion Chromatography-Small-Angle X-ray Scattering). This proof-of-concept application confirmed the possibility to develop simple biosensing tools at poly(Py-2-COOH) modified G-SPE for small molecules detection, such as PFOA. This detection strategy for PFOA, based on protein bioreceptor, offers two main advantages over the already reported electrochemical biosensors: it is label-free, not requiring any label or co-reactant to perform the detection and has the potential to be an easy, fast and robust method of fabrication, based on disposable screen printed electrode and not requiring complex instrumentations or time consuming modification protocols.

2. Materials and methods

Pyrrole-2-carboxylic acid (99%) (Py-2-COOH), perfluorooctanoic acid (PFOA, ≥96%), perfluorooctanesulfonic acid potassium salt (PFOS, ≥98%) and hydroxylamine were purchased from Sigma–Aldrich Ltd (Belgium). 1-ethyl-3-(3-dimethylamino) propyl carbodiimide hydrochloride (EDC) and N-hydroxysulfosuccinimide (NHS) were purchased from TCI (Europe). Highly purified delipidated human serum albumin (hSA) was obtained following the protocol reported in [36]. All the other reagents were of analytical grade and used as received. The 0.1 M phosphate buffer saline pH 7.4 with 0.01 NaCl was prepared by mixing stock solutions of 0.1 M NaH_2PO_4 and 0.1 M Na_2HPO_4, purchased form Sigma Aldrich. All aqueous solutions were prepared using MilliQ water (R > 18 MΩ cm). Electrochemical impedance spectroscopy (EIS) and cyclic voltammetry (CV) measurements were performed using an Autolab potentiostat/galvanostat (PGSTAT 302N, ECOCHEMIE, The Netherlands) controlled by NOVA 1.1 software. Disposable graphite screen-printed electrodes (G-SPE) consisting of a graphite working (3 mm diameter) and counter electrode and a silver pseudo reference electrode were purchased from Italsens (Florence, Italy).

2.1. G-SPE Py-2-COOH modification and characterization

The electropolymerization of 10 mM Py-2-COOH was performed by CV, using the following parameters: a potential window between −0.3 V and +1.2 V, at different scan rates (25, 50, 100 mV/s) and number of cycles (5, 10, 20). Two different electrolytes were tested namely 1 M $NaClO_4$ and 0.1 M SDS, both in aqueous solution. EIS measurements were recorded in 0.1 M phosphate buffer pH 7.4 with 2 mM $[Fe(CN)_6]^{3-/4-}$, in the frequency range between 0.1 MHz and 0.1 Hz, with 0.01 V amplitude and bias potential determined by open circuit potential. The EIS data were verified for linearity with the Kramers-Kronig transformation [37,38] and analysed using ZView 2. Except where otherwise stated, all the potentials are referred to silver pseudo reference electrodes (-200 mV compared to SCE). All electrochemical experiments were performed at room temperature. The modified and bare G-SPE morphology was characterized by scanning electron microscopy (SEM). SEM images were acquired with a Field Emission Gun – Environmental Scanning Electron Microscope equipped with an Energy Dispersive X-Ray detector (FEI Quanta 250, USA).

2.2. Covalent immobilization of hSA bioreceptor

A volume of 50 μL of 10 mM Py-2-COOH in 0.1 M SDS aqueous solution was placed on the G-SPE and the electropolymerization was performed by CV (5 cycles at 100 mV/s). The modified G-SPE were first rinsed with 1 mL phosphate buffer pH 7.4. To activate the carboxylic acid groups, 20 μL of an equimolar solution (0.07 M) of EDC/NHS in MilliQ water were incubated at the working electrode for 20 min keeping the G-SPE at 4° C. The solution was removed and 30 μL of 2 mg/mL delipidated hSA in phosphate buffer pH 7.4 were let in contact with the working electrode for 30 min at 4° C. The hSA modified G-SPE were rinsed with 1 mL phosphate buffer pH 7.4 to remove the protein excess. Then, the unreacted carboxylic acid groups were blocked with 20 μL of 1 M hydroxylamine [39] incubation for 20 min at 4° C. After hSA immo-

bilization, the G-SPE were characterized by EIS before being incubated with PFOA solutions.

2.3. Analytical protocol for PFOA detection

The modified electrode (hSA-Py-2-COOH-G-SPE) was incubated with 20 μL of PFOA solution at different concentrations for 20 min at RT. After, the electrode was rinsed with 500 μL of phosphate buffer and EIS spectra were acquired in 80 μL of 2 mM $[Fe(CN)_6]^{3-/4-}$ in 0.1 M phosphate buffer. The calibration plot was built in the concentration range between 100 nM and 5 μM: the relevant analytical parameter ΔZ is defined as the difference in absolute impedance values, acquired at 10 Hz, between the bare hSA-Py-2-COOH-G-SPE and after the incubation with PFOA. All measurements were performed in triplicates, unless otherwise indicated.

2.4. Size exclusion chromatography and small-angle X-ray scattering (SEC-SAXS)

The SEC-SAXS experiments were performed at the P12 beamline EMBL SAXS-WAXS at PETRAIII/DESY (Hamburg, Germany) [40]. The size exclusion chromatography (SEC) column (Superdex 200 5/150 column; GE Healthcare Life Sciences) was equilibrated with SEC-SAXS running buffer A (10 mM sodium phosphate, pH 7.4, 100 mM NaCl, 5% glycerol). A 50 μL aliquot of delipidated hSA (9 mg/mL) was applied to the column. The SEC column was then equilibrated with SEC-SAXS running solution B (buffer A plus 1 mM PFOA). Before performing the SAXS experiments on the complex, the delipidated hSA was pre-incubated with 1 mM PFOA for 30 min at room temperature and a 50 μL aliquot (9 mg/mL) was applied to the column. For each run 720 images were recorded using 1 s exposure every 1.25 s at a flow rate of 0.3 mL/min. For SEC-SAXS data, frames corresponding to delipidated hSA protein peak were identified, blank subtracted and averaged using CHROMIXS [41]. Radii of gyration (Rg), molar mass estimates and distance distribution functions P(r) were computed using the ATSAS package [42], in PRIMUS [43]. Comparison of experimental SAXS data (see Table S.M. 1) and delipidated hSA crystal structure (PDB_ID: 4K2C) [44] was performed using CRYSOL [45].

3. Results and discussion

3.1. Electropolymerization optimization

Surface modifications of screen printed electrodes may represent a challenging task and often protocols optimized for other type of electrodes (i.e. bulk macroelectrodes) are not directly compatible with SPE [46]. Modification protocols for SPE have to be straightforward and fast, while maintaining the performances of the bulk macro electrodes. In this study, the monomer electropolymerization was carried out by CV in aqueous solution avoiding organic solvents that might affect the stability of G-SPE coatings. Taking advantage on the wealth of information already present in literature only two electrolytes were tested, representing organic and inorganic anions: $NaClO_4$ [32] and SDS [33,34]. The use of these two electrolytes was linked to the good conductivity and stability of the final poly-pyrrole films obtained. Thus, they were considered the most suited candidates for the optimization of a robust poly(Py-2-COOH) film. All the parameters tested, namely number of cycles and scan rates, were evaluated in terms of final conductivity of the obtained film as well as duration of the modification protocol and applicability.

3.1.1. SDS versus $NaClO_4$

The electropolymerization of 10 mM Py-2-COOH at G-SPE was performed in 1 M of $NaClO_4$ [32] and in 0.1 M SDS [33,34] by running five CV cycles at 100 mV/s. The electropolymerization patterns reported in Fig. 1A and B showed a consistent behaviour for both electrolytes: the monomer oxidation occurred at about +1.1/1.2 V and the intensity of the peak current decreased with increasing the number of CV cycles. The peak currents were comparable for both $NaClO_4$ and SDS (≈400 μA for the first cycle) and the electrolytes differ mainly for the oxidation peak shape (more symmetrical and resolved for $NaClO_4$ solutions) and capacitive contribution (higher for SDS solution). However, the electrochemical properties of the modified electrodes investigated by CV and EIS were found to be completely different in terms of surface conductivity. In Fig. 1C, the voltammograms recorded in 2 mM $[Fe(CN_6)]^{3-/4-}$ 0.1 M KNO_3 for bare and poly(Py-2-COOH) modified G-SPE are compared. The electropolymerization in $NaClO_4$ (blue curve in Fig. 1C) passivate the electrode surface. The films obtained in SDS (red curve in Fig. 1C) showed a current increase of about 15% for both anodic and cathodic peaks and a smaller ΔEp (from 202 mV to 112 mV) compared to the bare G-SPE (black curve in Fig. 1C) both indications of enhanced electron transfer. The striking difference in conductivity of films obtained with the two modification protocols was confirmed by EIS, as showed in Fig. 1D. The electrode modified in $NaClO_4$ solution (blue dots in Fig. 1D) presented a very high charge transfer resistance (Rct) compared to the bare (black dots in Fig. 1D) as evidenced by the large semicircle in the Nyquist plot. This suggests the formation of a more insulating polymer-solution interface. On the contrary, the SDS modified electrode presents a Rct lower than the bare G-SPE, as underlined in Fig. 1E (red dots).

Therefore, it is possible to conclude that Py-2-COOH electropolymerization in aqueous solutions is compatible with G-SPE electrodes and the polymer properties can be easily tuned using different electrolytes. In particular, the use of $NaClO_4$ leads to insulating modifiers, while with SDS the poly(Py-2-COOH) is much more conductive. Moreover, the use of different electrolytes implies also slightly different polymer morphologies and distributions, as indicated by the SEM images reported in Fig. S.M. 1. Aiming to design a sensitive impedimetric platform, further optimization was performed only with the 0.1 M SDS electropolymerization solution.

3.1.2. Number of cycles and scan rate

The electropolymerization with SDS was optimized in terms of number of CV cycles and scan rate using a one-variable-at-a-time approach. The monomer solution, 10 mM of Py-2-COOH in 0.1 M SDS, was polymerized using increasing number of cycles (5, 10, 20) and different scan rates (25, 50, 100 mV/s). For studying the number of cycles, the scan rate was kept constant (100 mV/s) and five cycles of CV were recorded for each different scan rate value. The properties of all the modified G-SPE were characterized by CV and EIS in presence of 2 mM $[Fe(CN_6)]^{3-/4-}$, 0.1 M KNO_3.

Comparing the performances of the G-SPE modified at different number of cycles in Fig. 2A–B, it was possible to observe that the poly(Py-2-COOH) modification resulted in an higher surface conductivity compared to bare G-SPE even after 20 consecutive CV cycles. However, the best performances in terms of current intensities and ΔEp were obtained with five CV cycles (see Table S.M. 2). Increasing two or four times the number of CV cycles, there was an increment in ΔEp (from 112 mV for 5 cycles to 173 mV for the 20 cycles). To operate a rapid modification protocol, a number of five CV cycles was consider optimal for this study.

An even lower impact on the modified electrode performances was reported using different scan rates. The results presented in

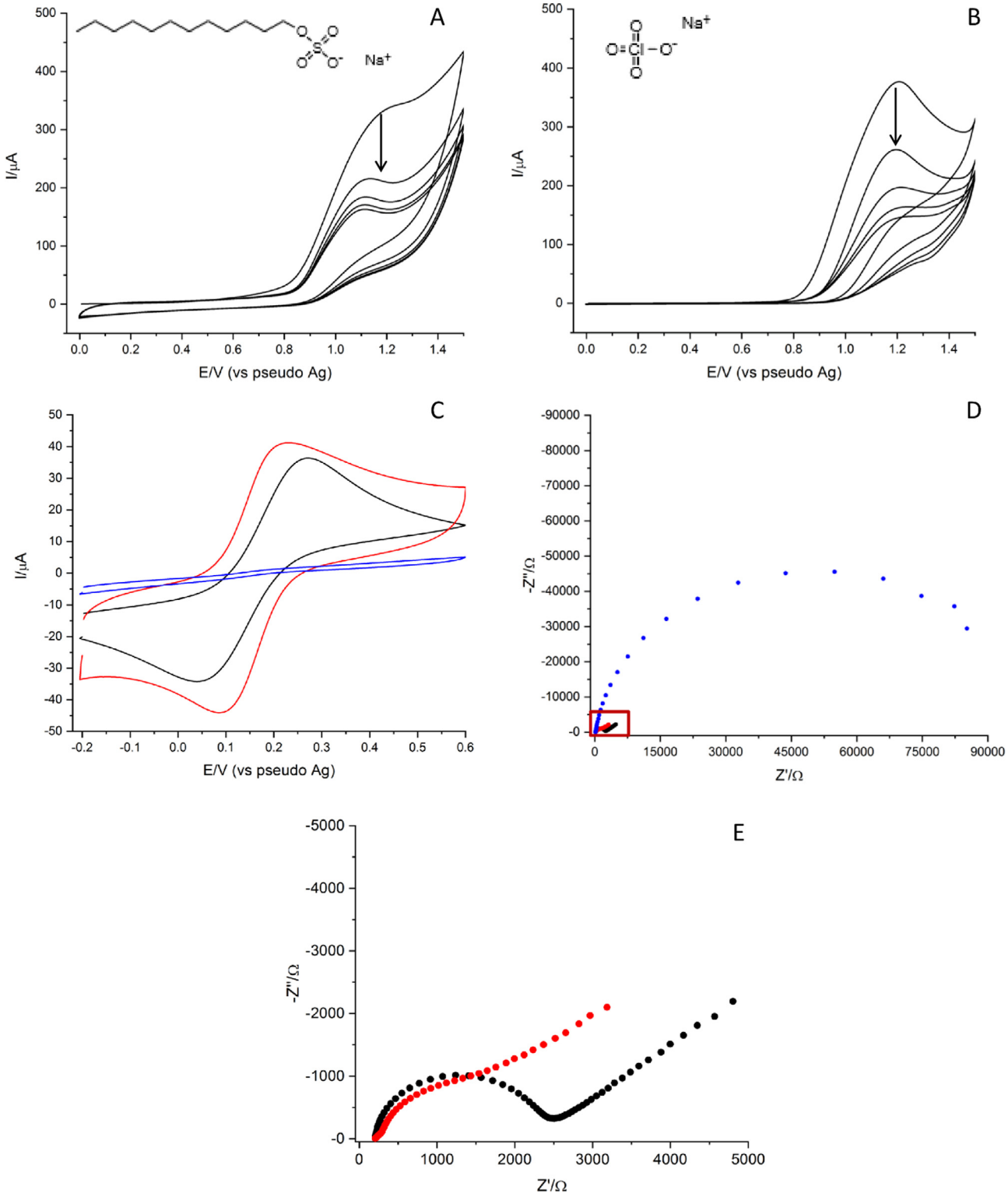

Fig. 1. Comparison of different electropolymerization patterns for 10 mM Py-2-COOH, 5 cycles at 100 mV/s between 0 and +1.5 V in 0.1 M SDS (A) and 1 M $NaClO_4$ (B); C) CVs for bare G-SPE (black line), and after 5 cycles of electropolymerization with 10 mM Py-2-COOH in 0.1 M SDS (red line) and 1 M $NaClO_4$ (blue line); D) Nyquist plot for bare G-SPE (black dots), and after 5 cycles of electropolymerization with 10 mM Py-2-COOH in 0.1 M SDS (red dots) and 1 M $NaClO_4$ (blue dots); E) Magnification of Nyquist plot in Fig. 1D (region from 0 to 5000 Ω). All the measurement were performed in 0.1 M KNO_3 with 2 mM $[Fe(CN_6)]^{3-/4-}$. (For interpretation of the references to colour in this figure legend, the reader is referred to the web version of this article.)

Fig. 2C showed a consistent behaviour with current variations of ±11% and ΔEp differences of maximum 22 mV (data overview in Table S.M. 2). To minimize the protocol duration, a scan rate value of 100 mV/s was finally selected. The slightly better performances of the electrodes modified with shorter protocols (5 cycles at 100 mV/S) might be explained by the polymerization solution. Indeed, the SDS solution has a very low surface tension and tend to spread on the electrode surface. Longer electropolymerization

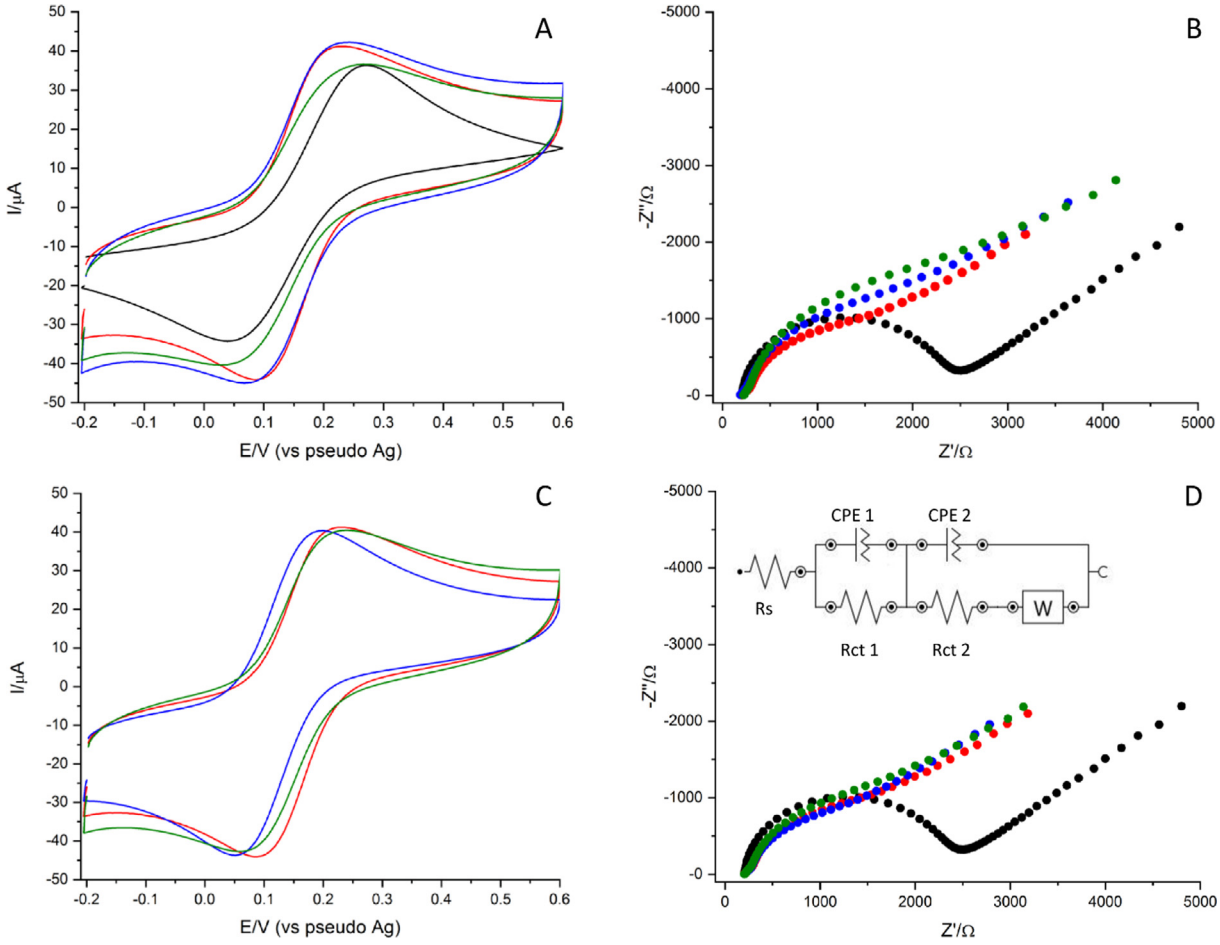

Fig. 2. Comparison of different electropolymerization parameters for 10 mM Py-2-COOH in 0.1 M SDS: CVs (A) and Nyquist plots (B) of G-SPEs after 5, 10 and 20 CV electropolymerization cycles at 100 mV/s; CVs (C) and Nyquist plots (D) of G-SPEs after 5 CV cycle electropolymerization at 25, 50 and 100 mV/s; inset: schematic representation of the electrochemical equivalent circuit used to fit the data. All the measurement were performed in 0.1 M KNO_3 with 2 mM $[Fe(CN_6)]^{3-/4-}$.

times might result in an uneven deposition since the monomer has more time to diffuse away from the WE surface.

The EIS data proved once again that the modified electrodes are still very conductive and indirectly report the successful modification of the electrode surface. The Nyquist plot for the modified electrodes can be fitted by the electrochemical equivalent circuit (EEC) reported as an inset in Fig. 2D. Two blocks of circuit elements can be identified; Rs is the uncompensated solution resistance while the first block [CPE 1, Rct 1] models the poly(Py-2-COOH) film and the second [CPE 2 (Rct 2 W)] is related to the electrode surface underneath the polymer. This circuit has been previously reported as a model for electrodes modified with materials with different conductivities and morphology of the underlying working electrode [47–49]. Thus, the final modification protocol encompass the electropolymerization of 10 mM of Py-2-COOH in 0.1 M SDS for 5 CV cycles at 100 mV/s. The resulting polymeric film provides the carboxylic acid functional groups needed for the covalent immobilization of biomolecules and improves the conductivity of the working electrode, as evidenced also by the EIS characterization.

3.2. Impedimetric characterization of hSA-PFOA binding

The possibility to follow the formation of the hSA-PFOA complex was investigated by EIS at the surface of the modified G-SPE. The electrode surface rich in carboxylic acid functionalities was activated by EDC/NHS for the covalent immobilization of delipidated hSA. The chosen immobilization protocol was developed specifically for application at G-SPE, as previously reported by Rengaraj *et al.* [39]. Preliminary test showed that the optimal hSA loading was achieved with a 2 mg/mL solution (as reported in Fig. S.M. 4). Then, different concentration of PFOA were let in contact with the hSA-modified electrodes prior to characterizing the changes in the surface properties by EIS.

3.2.1. Characterization of the hSA-Py-2-COOH modified G-SPE

The Nyquist plots obtained at the bare G-SPE (bare, black dots) and after Py-2-COOH electropolymerization (Py-2-COOH, red dots), delipidated hSA immobilization (hSA, blue dots) and PFOA incubation (PFOA 1 μM, green dots) are reported in Fig. 3. To extract qualitative and quantitative information about the processes occurring at the electrode surface, the Nyquist plots were fitted with EEC reported in Fig. 3B and C.

The Nyquist plot for the bare G-SPE was fitted with the modified Randles circuit, reported in Fig. 3B. In this circuit, the migration of charge through the electrolyte solution is described by the solution resistance (Rs), the double-layer formation at the electrode surface is modelled by a constant phase element (CPE), the charge-transfer reaction at the electrode corresponds to the Rct, and the linear diffusion from the bulk of the solution is modelled by the Warburg impedance element (W). The bare G-SPE presented a relatively high Rct (2.12 kΩ). After the electropolymerization of the conductive pyrrole-2-carboxylic acid film, the Rct was halved (1.02 kΩ). Moreover, the polymeric layer resulted to be highly reproducible and even G-SPEs with different initial Rct values showed compara-

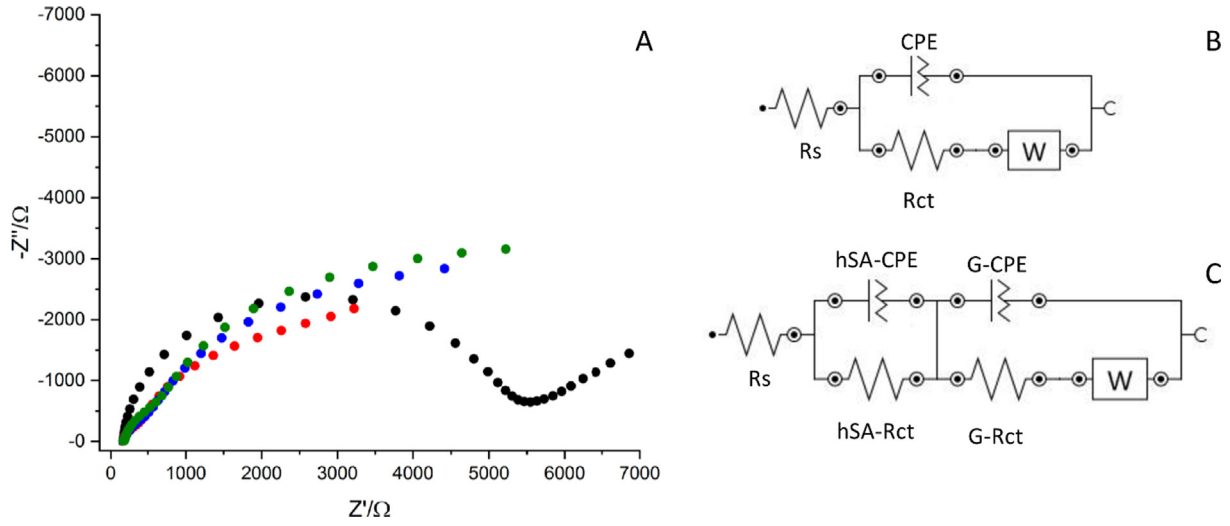

Fig. 3. (A) Nyquist plots for bare (black dots), poly(Py-2-COOH) modified G-SPE (red dots) and hSA poly(Py-2-COOH) modified G-SPE in absence (blue dots) and presence of 1 μM PFOA (green dots), (B) modified Randles EEC; C) hSA modified electrode EEC. All the measurement were performed in 0.1 M KNO_3 with 2 mM $[Fe(CN_6)]^{3-/4-}$. (For interpretation of the references to colour in this figure legend, the reader is referred to the web version of this article.)

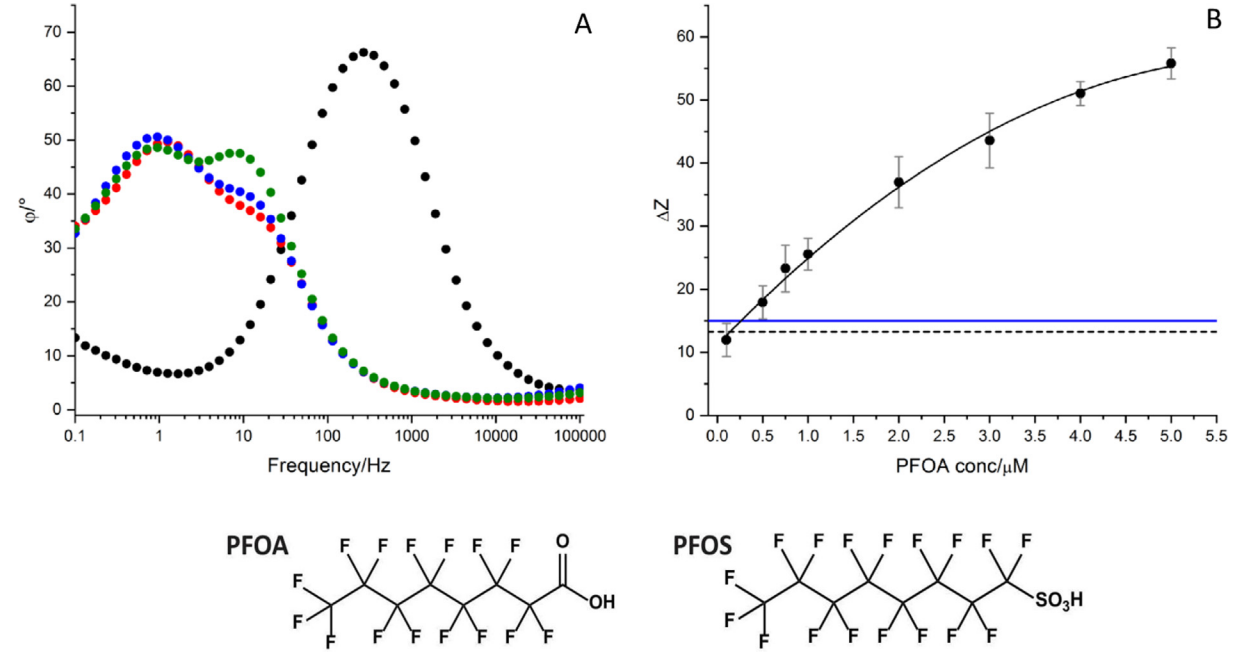

Fig. 4. (A) Bode phase plot for the hSA-Py-2-COOH-G-SPE recorded in 0.1 M phosphate buffer pH 7.4 with 2 mM $[Fe(CN_6)]^{3-/4-}$, bare (black dots), after Py-2-COOH electropolymerization (red dots), after hSA immobilization (blue dots) and after incubation with 1 μM PFOA (green dots); (B) Calibration plot for the hSA-Py-2-COOH-G-SPE biosensors between 100 nM and 5 μM PFOA, average signal for 5 incubations of pure buffer (dashed black line), average signal for 5 incubation of 1 μM PFOS solution (blue full line), polynomial fitting equation: $y = 11.20 + 14.97x^1 - 1.23x^2$. Error bars calculated on triplicates. Inset: PFOA (left) and PFOS (right) molecular structures. (For interpretation of the references to colour in this figure legend, the reader is referred to the web version of this article.)

ble performance after the electropolymerization. The immobilization of the delipidated hSA led to the formation of a conductive layer. To model this modification, a different EEC, reported in Fig. 3C, with an additional resistor and capacitor in parallel was used. A similar EEC was previously reported by Xie *et al.* in the EIS study of bovine serum albumin absorption at platinum electrodes [50]. The additional elements (hSA-CPE and hSA-Rct) model the resistance and capacitance of the conductive delipidated hSA film. Indeed, the charge must pass through the protein film before accessing the electrode surface (the part consisting of G-CPE, G-Rct and W). The Nyquist plot obtained after the incubation of 1 μM PFOA (green dots) presents an increase in the semicircle part of the plot at lower frequencies which is linked to an increase in Rct of the layer. Thus, it is possible to hypothesize a direct influence of the PFOA on the hSA structure on the electrode surface. The conformational changes of delipidated hSA in presence of PFOA were further investigated by SEC-SAXS. The results (reported in S.M. par. 2) suggest that PFOA compacts the structure of albumin leading to a meaningful decrease of the radius of gyration (Rg). However, it is worth to notice that no denaturation or protein unfolding was observed for hSA after incubation with PFOA. These data can be explained by considering the fatty-acid mimic beha-

viour of this contaminant that in presence of a completely delipidated protein is able to create strong interactions in the cavities that normally host lipids, hormones or drugs [51,52]. The structure assumed by the hSA in presence of PFOA might be responsible for the increase in Rct of the modified electrode; the redox mediator in solution will find its path towards the electrode surface hindered by the more compact hSA layer and thus resulting in an increased charge transfer resistance.

3.2.2. PFOA impedimetric analytical detection strategy

To simplify the detection strategy and improve the sensitivity of the sensors, a direct evaluation of the impedance signal changes was performed on the Bode phase plot instead of analysing the fitted parameters obtained from the EEC. From the Bode phase plot in Fig. 4A, recorded at the hSA-G-SPE (blue line), it was possible to identify two peaks, with Θ_{max} at 1 and 10 Hz, respectively. Each peak corresponds to a separate kinetic process with different time constants [53]. These processes were ascribed to the interaction of the redox mediator with the hSA and the polymeric film on the electrode surface. After incubation with PFOA containing solutions, the Θ_{max} of the process at 10 Hz increased (green line in Fig. 4A), suggesting that the presence of the contaminant changes the interaction between the hSA on the electrode surface and the redox mediator in solution. To use this event as analytical signal, the changes in the absolute impedance IZI [54], recorded at a fixed frequency of 10 Hz, were plotted against different PFOA concentrations, incubated at hSA-Py-2-COOH-G-SPE. The analytical parameter used is ΔZ, which is defined as the difference between the Z value of the hSA modified electrode at 10 Hz and the same value recorded after incubation with different PFOA solutions ($\Delta Z = |Z|_{PFOA} - |Z|_{hSA}$).

A calibration plot (Fig. 4B) was built in the range from 100 nM to 5 μM and the polynomial fitting of the data points had a R^2 of 0.997. PFOA concentrations higher than 2 μM result in the saturation of the bioreceptor. However, there is a possible linear interval between 500 nM and 2 μM. The error associated with the reproducibility of the impedimentric biosensors is c.a. 10%. As negative control tests, the hSA-G-SPE was incubated also with pure buffer (dashed black line in Fig. 4B) and 1 μM PFOS solution (full blue line in Fig. 4B). The average of 5 repeated measurements showed that the mean signals for both pure buffer and PFOS is lower then the value obtained with 500 nM of PFOA. The signal for 100 nM of PFOA falls below these threshold values and thus cannot be considered specific. These preliminary results showed the feasibility of an impedimetric-based PFOA detection strategy owing to its interactions with delipidated hSA.

4. Conclusion

Herein, the electropolymerization of a conductive poly(Py-2-COOH) modifier was optimized at G-SPE in 0.1 M SDS. The choice of this electrolyte assured reproducible and conductive polymer films on the screen-printed surface. Delipidated hSA was then covalently immobilized at the modified electrode via EDC/NHS coupling and the resulting modification was characterized by EIS. The obtained biosensing platform was tested in presence of increasing concentrations of PFOA and the changes at interfacial electron transfer were correlated to the formation of the hSA-PFOA complex. Extracting the absolute impedance values at 10 Hz from the Bode phase plot was possible to build a calibration plot in the nanomolar range. A possible interpretation of these impedimetric results was supported the study of the hSA-PFOA complex performed by SEC-SAXS analysis. This proof-of-concept study showed the ease of combining proteins bioreceptors with Py-2-COOH-G-SPE for PFOA monitoring in water samples. The applicability of this sensing strategy can be further improved by adding other surface electrode modifiers, such as nanomaterials or electroactive labels, to enhance the sensitivity or modifying the hSA receptor with protein engineering techniques.

Declaration of Competing Interest

The authors declare that they have no known competing financial interests or personal relationships that could have appeared to influence the work reported in this paper.

Acknowledgments

We gratefully acknowledge Gert Nuyts for the SEM measurements and FWO for funding the analytical equipment.

Appendix A. Supplementary data

Supplementary data to this article can be found online at https://doi.org/10.1016/j.bioelechem.2020.107540.

References

[1] G. Moro, K. De Wael, L.M. Moretto, Challenges in the electrochemical (bio) sensing of nonelectroactive food and environmental contaminants, Curr. Opin. Electrochem. 16 (2019) 57–65.
[2] X. Dauchy, Per- and polyfluoroalkyl substances (PFASs) in drinking water: Current state of the science, Curr. Opin. Environ. Sci. Heal. 7 (2019) 8–12.
[3] Y. Pan, J. Wang, L.W.Y. Yeung, S. Wei, J. Dai, Analysis of emerging per- and polyfluoroalkyl substances: Progress and current issues, TrAC, Trends Anal. Chem. (2019) 115481.
[4] S. Liu, R. Yang, N. Yin, Y.-L. Wang, F. Faiola, Environmental and human relevant PFOS and PFOA doses alter human mesenchymal stem cell self-renewal, adipogenesis and osteogenesis, Ecotoxicol. Environ. Saf. 169 (2019) 564–572.
[5] M. Zhang, P. Wang, Y. Lu, X. Lu, A. Zhang, Z. Liu, Y. Zhang, K. Khan, S. Sarvajayakesavalu, Bioaccumulation and human exposure of perfluoroalkyl acids (PFAAs) in vegetables from the largest vegetable production base of China, Environ. Int. 135 (2020) 105347.
[6] A. Cordner, V.Y. De La Rosa, L.A. Schaider, R.A. Rudel, L. Richter, P. Brown, Guideline levels for PFOA and PFOS in drinking water: the role of scientific uncertainty, risk assessment decisions, and social factors, J. Expo. Sci. Environ. Epidemiol. 29 (2019) 157–171.
[7] D. Banks, B.-M. Jun, J. Heo, N. Her, C.M. Park, Y. Yoon, Selected advanced water treatment technologies for perfluoroalkyl and polyfluoroalkyl substances: A review, Sep. Purif. Technol. 231 (2020) 115929.
[8] P.C. Ferreira, V.N. Ataíde, C.L. Silva Chagas, L. Angnes, W.K. Tomazelli Coltro, T. R. Longo Cesar Paixão, W. Reis de Araujo, Wearable electrochemical sensors for forensic and clinical applications, TrAC, Trends Anal. Chem. 119 (2019) 115622.
[9] L. Lu, Z. Zhu, X. Hu, Multivariate nanocomposites for electrochemical sensing in the application of food, TrAC Trends Anal. Chem. 118 (2019) 759–769.
[10] C. Fang, Z. Chen, M. Megharaj, R. Naidu, Potentiometric detection of AFFFs based on MIP, Environ. Technol. Innov. 5 (2016) 52–59.
[11] S. Chen, A. Li, L. Zhang, J. Gong, Molecularly imprinted ultrathin graphitic carbon nitride nanosheets–based electrochemiluminescence sensing probe for sensitive detection of perfluorooctanoic acid, Anal. Chim. Acta. 896 (2015) 68–77.
[12] J. Gong, T. Fang, D. Peng, A. Li, L. Zhang, A highly sensitive photoelectrochemical detection of perfluorooctanic acid with molecularly imprinted polymer-functionalized nanoarchitectured hybrid of AgI–BiOI composite, Biosens. Bioelectron. 73 (2015) 256–263.
[13] F. Cao, L. Wang, Y. Tian, F. Wu, C. Deng, Q. Guo, H. Sun, S. Lu, Synthesis and evaluation of molecularly imprinted polymers with binary functional monomers for the selective removal of perfluorooctanesulfonic acid and perfluorooctanoic acid, J. Chromatogr. A. 1516 (2017) 42–53.
[14] L. Zheng, Y. Zheng, Y. Liu, S. Long, L. Du, J. Liang, C. Huang, M.T. Swihart, K. Tan, Core-shell quantum dots coated with molecularly imprinted polymer for selective photoluminescence sensing of perfluorooctanoic acid, Talanta. 194 (2019) 1–6.
[15] N. Cennamo, L. Zeni, P. Tortora, M.E. Regonesi, A. Giusti, M. Staiano, S. D'Auria, A. Varriale, A high sensitivity biosensor to detect the presence of perfluorinated compounds in environment, Talanta. 178 (2018) 955–961.
[16] X. Liu, M. Fang, F. Xu, D. Chen, Characterization of the binding of per- and polyfluorinated substances to proteins: A methodological review, TrAC Trends Anal. Chem. 116 (2019) 177–185.
[17] M. Salvalaglio, I. Muscionico, C. Cavallotti, Determination of energies and sites of binding of PFOA and PFOS to human serum albumin, J. Phys. Chem. B. 114 (2010) 14860–14874.

[18] Q. Chi, Z. Li, J. Huang, J. Ma, X. Wang, Interactions of perfluorooctanoic acid and perfluorooctanesulfonic acid with serum albumins by native mass spectrometry, fluorescence and molecular docking, Chemosphere 198 (2018) 442–449.
[19] C. He, M. Xie, F. Hong, X. Chai, H. Mi, X. Zhou, L. Fan, Q. Zhang, T. Ngai, J. Liu, A highly sensitive glucose biosensor based on gold nanoparticles/bovine serum albumin/Fe3O4 biocomposite nanoparticles, Electrochim. Acta. 222 (2016) 1709–1715.
[20] Z. Tang, Y. Fu, Z. Ma, Bovine serum albumin as an effective sensitivity enhancer for peptide-based amperometric biosensor for ultrasensitive detection of prostate specific antigen, Biosens. Bioelectron. 94 (2017) 394–399.
[21] J.S. Daniels, N. Pourmand, Label-free impedance biosensors: opportunities and challenges, Electroanalysis. 19 (2007) 1239–1257.
[22] F. Ghorbani Zamani, H. Moulahoum, M. Ak, D. Odaci Demirkol, S. Timur, Current trends in the development of conducting polymers-based biosensors, TrAC, Trends Anal. Chem. 118 (2019) 264–276.
[23] M.H. Naveen, N.G. Gurudatt, Y.B. Shim, Applications of conducting polymer composites to electrochemical sensors: A review, Appl. Mater. Today. 9 (2017) 419–433.
[24] A.C. Gálvez-Iriqui, M.O. Cortez-Rocha, A. Burgos-Hernández, M. Calderón-Santoyo, W.M. Argüelles-Monal, M. Plascencia-Jatomea, Synthesis of chitosan biocomposites loaded with pyrrole-2-carboxylic acid and assessment of their antifungal activity against Aspergillus niger, Appl. Microbiol. Biotechnol. 103 (2019) 2985–3000.
[25] J. Qin, D.G. Jo, M. Cho, Y. Lee, Monitoring of early diagnosis of Alzheimer's disease using the cellular prion protein and poly(pyrrole-2-carboxylic acid) modified electrode, Biosens. Bioelectron. 113 (2018) 82–87.
[26] A. Kausaite-Minkstimiene, L. Glumbokaite, A. Ramanaviciene, E. Dauksaite, A. Ramanavicius, An amperometric glucose biosensor based on poly (pyrrole-2-carboxylic acid)/glucose oxidase biocomposite, Electroanalysis. 30 (2018) 1634–1644.
[27] M. Foschini, H.S. Silva, R.A. Silva, A. Marletta, D. Gonçalves, Theoretical and experimental studies on the electronic, optical, and structural properties of poly-pyrrole-2-carboxylic acid films, Chem. Phys. 425 (2013) 91–95.
[28] G. Sabouraud, S. Sadki, N. Brodie, The mechanisms of pyrrole electropolymerization, Chem. Soc. Rev. 29 (2002) 283–293.
[29] G.K. Chandler, D. Pletcher, The electrodeposition of metals onto polypyrrole films from aqueous solution, J. Appl. Electrochem. 16 (1986) 62–68.
[30] T.F. Otero, J. Rodríguez, Parallel kinetic studies of the electrogeneration of conducting polymers: mixed materials, composition and properties control, Electrochim. Acta. 39 (1994) 245–253.
[31] L.F. Warren, D.P. Anderson, Polypyrrole films from aqueous electrolytes: the effect of anions upon order, J. Electrochem. Soc. 134 (1987) 101–105.
[32] Y. Li, J. Yang, Effect of electrolyte concentration on the properties of the electropolymerized polypyrrole films, J. Appl. Polym. Sci. 65 (2002) 2739–2744.
[33] J.M. Pernaut, R.C.D. Peres, V.F. Juliano, M.-A. De Paoli, Electrochemical study of polypyrrole/dodecyl sulphate, J. Electroanal. Chem. Interfacial Electrochem. 274 (1989) 225–233.
[34] D.-H. Han, H.J. Lee, S.-M. Park, Electrochemistry of conductive polymers XXXV: Electrical and morphological characteristics of polypyrrole films prepared in aqueous media studied by current sensing atomic force microscopy, Electrochim. Acta. 50 (2005) 3085–3092.
[35] H. Chen, P. He, H. Rao, F. Wang, H. Liu, J. Yao, Systematic investigation of the toxic mechanism of PFOA and PFOS on bovine serum albumin by spectroscopic and molecular modeling, Chemosphere. 129 (2015) 217–224.
[36] R.F. Chen, Removal of fatty acids from serum albumin by charcoal treatment, J. Biol. Chem. 242 (1967) 173–181.
[37] B.A. Boukamp, Practical application of the Kramers-Kronig transformation on impedance measurements in solid state electrochemistry, Solid State Ion. 62 (1993) 131–141.
[38] P. Agarwal, M.E. Orazem, L.H. Garcia-Rubio, Application of measurement models to impedance spectroscopy III. Evaluation of consistency with the Kramers-Kronig relations, J. Electrochem. Soc. 142 (1995) 4159–4168.
[39] S. Rengaraj, Á. Cruz-Izquierdo, J.L. Scott, M. Di Lorenzo, Impedimetric paper-based biosensor for the detection of bacterial contamination in water, Sens. Actuat. B Chem. 265 (2018) 50–58.
[40] C.E. Blanchet, A. Spilotros, F. Schwemmer, M.A. Graewert, A. Kikhney, C.M. Jeffries, D. Franke, D. Mark, R. Zengerle, F. Cipriani, S. Fiedler, M. Roessle, D.I. Svergun, Versatile sample environments and automation for biological solution X-ray scattering experiments at the P12 beamline (PETRA III, DESY), J. Appl. Crystallogr. 48 (2015) 431–443.
[41] A. Panjkovich, D.I. Svergun, CHROMIXS: Automatic and interactive analysis of chromatography-coupled small-angle X-ray scattering data, Bioinformatics. 34 (2018) 1944–1946.
[42] D. Franke, M.V. Petoukhov, P.V. Konarev, A. Panjkovich, A. Tuukkanen, H.D.T. Mertens, A.G. Kikhney, N.R. Hajizadeh, J.M. Franklin, C.M. Jeffries, D.A. Svergun, ATSAS 2.8: A comprehensive data analysis suite for small-angle scattering from macromolecular solutions, J. Appl. Crystallogr. 50 (2017) 1212–1225.
[43] P.V. Konarev, V.V. Volkov, A.V. Sokolova, M.H.J. Koch, D.I. Svergun, PRIMUS: A Windows PC-based system for small-angle scattering data analysis, J. Appl. Crystallogr. 36 (2003) 1277–1282.
[44] Y. Wang, H. Yu, X. Shi, Z. Luo, D. Lin, M. Huang, Structural mechanism of ring-opening reaction of glucose by human serum albumin, J. Biol. Chem. 288 (2013) 15980–15987.
[45] D. Svergun, C. Barberato, M.H. Koch, CRYSOL - A program to evaluate X-ray solution scattering of biological macromolecules from atomic coordinates, J. Appl. Crystallogr. 28 (1995) 768–773.
[46] G. Moro, D. Cristofori, F. Bottari, E. Cattaruzza, K. De Wael, M.L. Moretto, Redesigning an Electrochemical MIP Sensor for PFOS: Practicalities and Pitfalls, Sensors. 19 (2019) 4433.
[47] A. Ramanavicius, A. Finkelsteinas, H. Cesiulis, A. Ramanaviciene, Electrochemical impedance spectroscopy of polypyrrole based electrochemical immunosensor, Bioelectrochemistry. 79 (2010) 11–16.
[48] C. Deslouis, M.M. Musiani, B. Tribollet, Free-standing membranes for the study of electrochemical reactions occurring at conducting polymer/electrolyte interfaces, J. Phys. Chem. 100 (1996) 8994–8999.
[49] M.A. Vorotyntsev, B. Tribollet, Comparison of the AC impedance of conducting polymer films studied as electrode-supported and freestanding membranes, J. Electrochem. Soc. 142 (1995) 1902–1908.
[50] Q. Xie, C. Xiang, Y. Yuan, Y. Zhang, L. Nie, S. Yao, A novel dual-impedance-analysis EQCM system—investigation of bovine serum albumin adsorption on gold and platinum electrode surfaces, J. Colloid Interface Sci. 262 (2003) 107–115.
[51] J. Ghuman, P.A. Zunszain, I. Petitpas, A.A. Bhattacharya, M. Otagiri, S. Curry, Structural basis of the drug-binding specificity of human serum albumin, J. Mol. Biol. 353 (2005) 38–52.
[52] A.A. Bhattacharya, T. Grüne, S. Curry, Crystallographic analysis reveals common modes of binding of medium and long-chain fatty acids to human serum albumin, J. Mol. Biol. 303 (2000) 721–732.
[53] E. Casero, A.M. Parra-Alfambra, M.D. Petit-Domínguez, F. Pariente, E. Lorenzo, C. Alonso, Differentiation between graphene oxide and reduced graphene by electrochemical impedance spectroscopy (EIS), Electrochem. Commun. 20 (2012) 63–66.
[54] Vadim F. Lvovich (Ed.), Impedance Analysis of Complex Systems, in: Impedance Spectrosc., 2012, pp. 113–161.